RSC Advances

PAPER

View Article Online
View Journal | View Issue

Cite this: *RSC Adv.*, 2016, **6**, 3778

Ripening and recrystallization of NaCl nanocrystals in humid conditions†

M. Oliva-Ramirez, M. Macías-Montero,‡ A. Borras and A. R. González-Elipe*

This study shows that Ostwald ripening, a universal mechanism responsible for the increase of crystal size during precipitation from solutions, can be meditated by ion diffusion through condensed monolayers of water that connect separated nanocrystals. In an environmental electron microscope we have observed "*in situ*" the time evolution of the number, shape, size and crystallographic texture of NaCl nanoparticles deposited by electron beam evaporation at oblique angles. Analysis of NaCl nanoparticles before and after water vapor condensation has evidenced that the size of nanocrystals is not the unique driving force inducing nanoparticle ripening and recrystallization, but the faceting of their crystalline habits and the amorphisation degree of the initially deposited nuclei also play important roles. These findings have implications for other crystallization and nucleation processes and can be of relevance for rock weathering and related phenomena.

Received 26th October 2015
Accepted 17th December 2015

DOI: 10.1039/c5ra22425j

www.rsc.org/advances

Introduction

Ostwald ripening is a universal coarsening phenomenon occurring during crystallization in solutions[1–3] and in other systems such as water droplets[4,5] or emulsions,[6] which leads to the size increase of nuclei bigger than a critical value (*i.e.* critical nucleation size d_c) at the expense of those with a smaller size.[7] This phenomenon has been recursively studied at a fundamental level[2,8–14] and technologically applied to control the crystal size distribution in precipitates, tune the hollow microstructure of nanostructured materials or to grow nanostructures with well selected sizes and shapes.[15–17] According to the original proposals of Ostwald,[18] ripening is driven by the size dependence of the surface to bulk energy ratio and requires a dispersive medium that enables material diffusion among nuclei.

In nature, geological precipitation of crystals,[19,20] rock weathering[21] or ice formation in the troposphere[22] can be mediated by Ostwald ripening after the dissolution of salt precipitates in rain or surface condensed water. Dissolution phenomena considering the effect of condensed layers of water on single crystals and other model systems have been monitored "*in situ*" by AFM,[23] environmental XPS[23–25] or TEM.[26] Herein, the ripening process occurring in a multi-nuclei NaCl system has been directly monitored under an environmental scanning electron microscope (ESEM) wherein water vapour pressure was increased up to saturation. Under these conditions, we followed the time evolution of the number, size and shapes of the salt nanoparticles and found some unexpected clues determining their transformation. This "*in situ*" ESEM investigation has been complemented with "*in situ*" and "*ex situ*" X-ray diffraction analysis to verify possible modifications in crystalline structure. For this study, we have evaporated NaCl using an electron beam in an oblique angle deposition (OAD) configuration (also known as glancing angle deposition, GLAD)[27,28] onto Si(100) wafer substrates. This geometrical arrangement offers invaluable possibilities of microstructure control that had not been explored before with NaCl, even if thin films of this material have been recurrently deposited by physical vapour deposition in a normal configuration.[29–31] Evaporation at oblique angles promotes the appearance of shadowing effects during deposition and leads to the initial formation of isolated nuclei and the subsequent growth of thin films with an open and tilted columnar nanostructure.[27,28,32,33] By controlling different deposition parameters, particularly the zenithal angle of deposition (*i.e.* angle formed between the NaCl evaporated flux and the axis perpendicular to the substrate surface), we have been able to control the size, shape and connectivity of the initially formed NaCl nuclei. Ripening results have been shown for selected samples deposited at zenithal angles of 60° and 85° (hereafter named as NaCl-60° and NaCl-85°).

Results and discussion

Nanoparticle morphology and crystallographic structure

Fig. 1 shows a series of normal SEM images and the XRD patterns obtained for the as-prepared NaCl-60° and -85° samples. In the former, the salt nanoparticles appear

Nanotechnology on Surfaces Laboratory, Instituto de Ciencia de Materiales de Sevilla (CSIC-Univ. Sevilla), 41092 Sevilla, Spain. E-mail: arge@icmse.csic.es

† Electronic supplementary information (ESI) available. See DOI: 10.1039/c5ra22425j

‡ Present address: Plasma Non-synthesis & Solar Cell Devices, Engineering Research Institute, University of Ulster, Jordanstown campus, Shore Road Newtownabbey, Co. Antrim, BT370QB, UK.

interconnected and present rounded-edge profiles, whereas its diffraction pattern taken in a Bragg–Brentano configuration reveals a texture where the (220) planes are parallel to the substrate surface. By contrast, the NaCl-85° sample is formed by isolated nuclei. The tendency towards the formation of isolated nanoparticles in NaCl-85° is due to an enhancement of shadowing effects at this deposition angle. The lack of intense diffraction peaks in this sample sustains a poor crystalline order with a limited number of particles with well-defined and defect-free (200) and (220) planes parallel to the substrate surface. It also agrees with the amorphisation tendency expected for materials deposited under ballistic conditions during OAD (*e.g.*, at room temperature and oblique angles) that preclude the surface diffusion of ad-particles.[34,35] We will observe later that this poor crystallization degree and/or heterogeneous crystalline character of nanoparticles may have important effects on the ripening process.

"*In situ*" SEM observation of ripening

Samples were introduced in the ESEM microscope wherein the temperature was brought down to *ca.* 8 °C before increasing the relative humidity up to a value close to 80% (a typical evolution of the relative humidity expressed in percentages is shown in Fig. 2D). After reaching these temperature and humidity values, the NaCl nanoparticles experienced progressive changes in shape and size that were monitored "*in situ*" under the microscope. These changes are evidenced by the series of successive electron micrographs obtained for *ca.* 15 min (shown in Fig. 2A) and the evaluation (reported in Fig. 2C) of the number and size distribution of nuclei directly deduced from the images. The plots in this figure reveal a decrease of *ca.* one third in the number of nuclei and a clear increase from sizes smaller than 0.3 μm in the initial state (*i.e.* image 1 in Fig. 2A) to the final situation (*i.e.* images 4 and 5 in Fig. 2A) with a considerable number of particles between 0.2 and 0.6 μm and large crystals of up to 1.5 μm, all this meaning an increase in average size from 0.06 to 0.16 μm during the whole ripening process. This analysis also revealed that the calculated total volume of salt, determined as Nd^3 (N is the number of particles in each case taken as cubic), is practically equivalent both before (39 000 μm^3) and after (33 300 μm^3) the ripening experiment. A rough estimate of particle distribution also showed that the average distance between the edges of nanoparticles varies from an initial value D_i of 0.47 μm to D_f of 0.74 μm in the final state. The observed evolution involves the complete dissolution of some nanoparticles and the increase in size of others, both processes occurring in parallel as clearly observed in the reported images. Phenomenologically, this behaviour is typical of an Ostwald ripening mechanism wherein the smallest nanoparticles dissolve and their constituent material is transferred to the growing particles. As we will discuss later, in this system, the

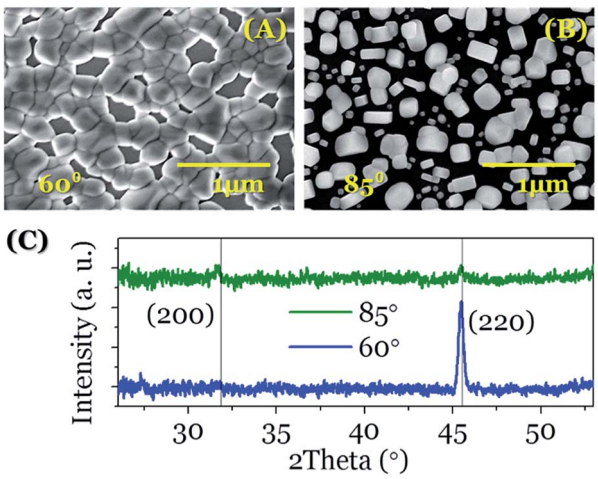

Fig. 1 NaCl nanoparticles prepared by e-beam evaporation at oblique angles. (top) Normal scanning electron micrographs of samples NaCl-60° (A) and NaCl-85° (B). The X-ray diffraction pattern of these nanocrystals is reported in (C).

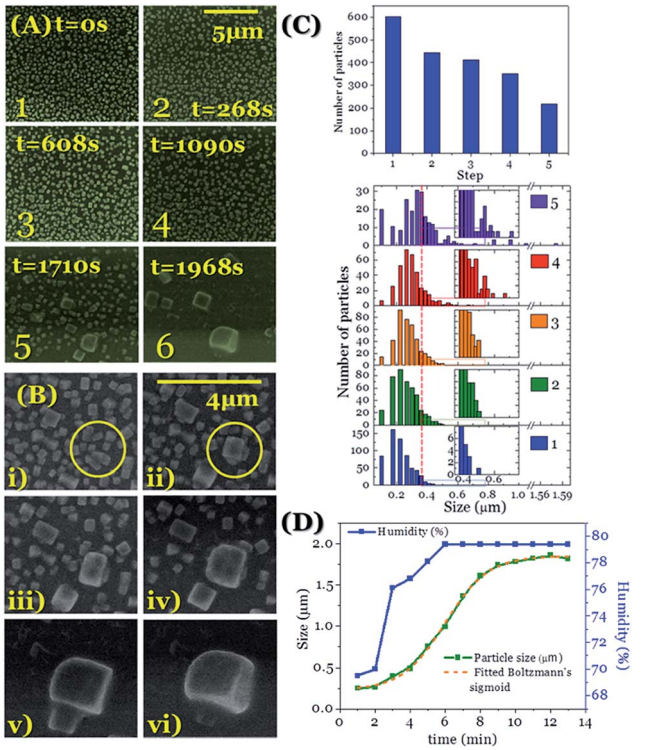

Fig. 2 Evolution of the number and particle size distribution of nanoparticles in sample NaCl-85° after exposure to a humid environment. (A) Normal SEM micrographs of the deposited NaCl nanoparticles taken at successive times as indicated. In panel 6 water condensation accompanied by the complete dissolution of the smallest crystallites can be observed. (B) Enlarged images of a selected zone monitoring the evolution of the nanoparticle reaching a maximum final size. (C) Plots of the number of nanoparticles and particle size distribution as a function of exposure time to water vapour. The inset plots with an expanded y-axis have been included to better visualize the evolution of the number of particles of larger size. (D) Evolution of the water pressure in the ESEM chamber as a function of time and plot of the size evolution of the nanoparticle selected in (B) (estimated from its projected area) to determine its growth kinetics. Superimposed onto the experimental curve is a fitting Boltzmann's sigmoidal curve. The onset of size increase at a maximum vapour pressure of approximately 440 Pa indicates the point at which water condenses and forms a continuous water layer on the sample surface.

ripening process may be driven by additional factors and the selection of particles that grow/dissolve might not only depend on size effects as in a classical Ostwald ripening mechanism.[18]

To get a deeper insight into the kinetics of this process, we closely followed the evolution of a nucleus experiencing the largest size increase within the observation area (*i.e.*, in this particular experiment, we selected the encircled nanoparticle in Fig. 2B). Fig. 2D shows that the function size *vs.* time $d(t)$ adopts a sigmoidal shape that can be fitted with a Sigmoidal Boltzmann Equation (SBE):[6]

$$d(t) = \frac{d_i - d_f}{1 + e^{(t-t_i)/\Delta t}} + d_i \quad (1)$$

where d_i and d_f are the initial and final sizes of the selected crystal, in this case taken for simplicity in one dimension as 0.23 and 1.85 μm, respectively. The parameter t_i represents the critical exposure time and corresponds to the inflexion point of the curve, *i.e.*, for $t < t_i$, the crystal grows at an increasing rate, whereas for $t > t_i$, the crystal growth rate decreases progressively until converging to its final size d_f. The growth period is described by Δt. In the present experiment, $t_i = 6.0$ min and $\Delta t = 12$ min, meaning that the whole ripening process occurs in *ca.* 12 min. A reasonable assumption is that the initial induction period of 6.0 min accounts for the time required for saturating a condensed water layer with Cl^- and Na^+ ions, in other words, to dissolve the external layers of the NaCl particles to reach steady-state ion diffusion conditions among nuclei. Within this scheme, the observed increasing rate of $\Delta d(t)$ in the first part of the ripening process relates to the short average distance of $D_i = 0.47$ μm existing between the targeted nanoparticle and the surrounding nuclei, all of them a net source of Cl^- and Na^+ ions. In the second part of the experiment (*i.e.* when $t > t_i$), the area surrounding the monitored nanoparticle becomes progressively depleted of these small nuclei, which are now separated by $D_f = 0.74$ μm; this implies that the growth process slows down to finally stop. In the final stage, salt dissolution and re-deposition compensate and the overall system reaches a stationary state. A similar evolution was also found for sample NaCl-60°, although the connected microstructure of NaCl nanoparticles in this sample precluded a quantitative analysis (see ESI S1†). The basic assumption of this ripening mechanism, *i.e.*, the migration of ions in a condensed layer of water was directly observed by Salmeron *et al.*[23–25] in an "*in situ*" environmental XPS and AFM study showing the partial dissolution of alkali halide single crystals and the incorporation of their constituent ions into the liquid layer.

Crystallization and facet evolution

To a first approximation, the phenomenology of the ripening described by eqn (1) might agree with a typical Ostwald process driven by particle size differences,[2,7–16] *i.e.*, the increase in size of the bigger particles at the expense of the smallest ones that disappear. However, a closer look of the results suggests that other factors besides size effects may be involved in the process. The XRD spectra in Fig. 3A taken for sample NaCl-60° before and after the ESEM experiments indicate that an increase in crystallization degree from an initially less crystalline state and a drastic change in the nanocrystals' plane texture from a (220) to a (200) preferential orientation occur in parallel with ripening. According to the schematic NaCl fcc unit cell drawings in Fig. 3C, the XRD-determined textural change implies a transformation of the external facets of nanoparticles, which after water vapour exposure would be terminated by (200) and equivalent family planes (*i.e.*, (020) and (002)). A similar evolution was also found for sample NaCl-85° (*cf.*, Fig. 3B), which changed from an initial state with (200) and (220) planes parallel to the substrate (the low intensity of these peaks suggests a poor crystallinity) to a final situation wherein a well-defined (200) peak proves a net evolution of both crystallinity and texture. The general character of this (220) to (200) textural transformation was confirmed in an "*in situ*" XRD experiment at 298 K for sample NaCl-60° exposed to water saturated air in the environmental chamber of the apparatus (see ESI S2†).

These crystallographic rearrangements determined by XRD run in parallel to changes in the shape and facet orientation of the nanoparticles. Fig. 4A and C show a series of successive cross-sectional ESEM micrographs taken for sample NaCl-60° at 40 s intervals once the ripening threshold conditions were reached. A video with the whole set of micrographs recorded during this experiment is presented as ESI (S3†). Besides a common change in the nanoparticles' shape from rounded- to cubic-edged form, a careful observation of selected nuclei (Fig. 4B) shows the disappearance of facets forming 45° angles with the substrate (in those cases where such facets can be observed in the rather rounded shapes of the initially deposited crystallites) and the progressive evolution of 90° and 180° oriented facets (*i.e.* perfect cubic shapes). Similar effects could be observed for sample NaCl-85° (Fig. 4D). These morphological changes together with the evolution of the XRD diagrams in Fig. 3, clearly demonstrate that a complete re-growing of nanoparticles occurs in parallel with their size increase by ripening.

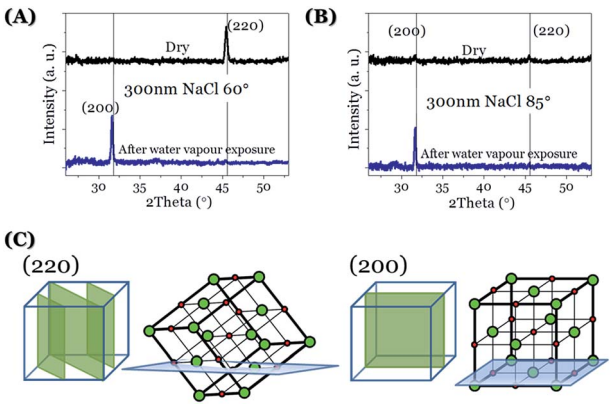

Fig. 3 Evolution of crystallographic structure of NaCl nanoparticles after exposure to 80% humidity. X-ray diffraction patterns of (A) sample NaCl-60° and (B) sample NaCl-85° before and after exposure to water vapour at 8 °C in the ESEM. (C) Representations of the crystal unit cell orientations of NaCl with respect to the substrate before (left) and after (right) exposure to water vapour.

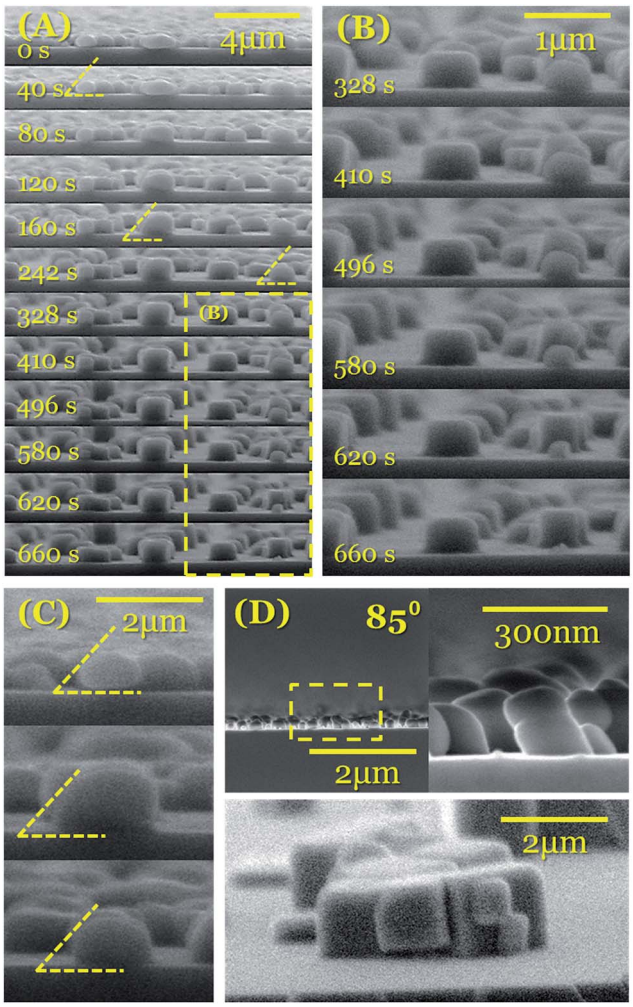

Fig. 4 Shape and facet modification of NaCl nanoparticles by exposure to saturated water vapour. (A) Cross-section ESEM micrographs taken for sample NaCl-60° exposed to water vapour for successive periods of time as indicated. (B) Enlarged views of some faceted nanoparticles. The tilted dashed lines highlight facets forming an angle of 45° with respect to the substrate. (C) Enlarged views of selected nanoparticles. (D) Micrographs corresponding to initial (top) and final (bottom) states taken during a similar experiment with sample NaCl-85°. A tilted morphology of the nanoparticles in the initial state is clearly visible in the enlarged micrograph on the right in this panel.

Ripening driving forces

The experimental results summarized in Fig. 1–4 require the dissolution and mobilization of Na^+ and Cl^- ions through a layer of water condensed on the nanoparticles and onto the free zones of the substrate that lead to a change in their number and size, which at first glance, seems to follow the surface to bulk energy premise of classical Ostwald ripening. However, the observed changes in texture and particle shapes (*i.e.* facet termination) indicate that other factors associated with the different stabilization energies of crystals and facet termination must contribute as additional driving forces to the transformation and rearrangement of the nanoparticles. The observed changes are presented as the schematic in Fig. 3: in the initial sate a majority of nanoparticles orient with their (220) planes parallel to the substrate, whereas some of them are terminated in (200) facets at 45° to the substrate surface. Regrowth of nanoparticles after water vapour exposure induces their rearrangement into a cubic crystalline structure with the (200) planes parallel to the substrate and termination in the crystallographically equivalent (200), (020) and (002) facets. (220) and (200) crystal faces of NaCl have ion densities[36] of 4.44 and 6.29 ions nm^{-2}, respectively, and, according to free-energy calculations by Mulheran,[37] surface energies of 160 and 267 mJ m^{-2}, respectively (note that these values should be taken with a negative sign if referred to as Gibbs free energies). This evolution of crystal facets upon ripening agrees with the classical Gibbs–Wulff postulates of equilibrium shapes of crystal growth (NaCl crystals are known to terminate in 100 facets) rather than with the Frank–Chernov principles of steady-state growth shapes.[38]

Besides particle size and facet termination, the partial amorphous character of the NaCl nuclei prepared by OAD must operate as an additional driving force for nanoparticle transformation and ripening. In fact, as suggested by the XRD analysis of sample NaCl-85°, nanoparticle ripening is accompanied by a net increase in crystallization degree, suggesting that more amorphous particles dissolve preferentially and/or that a partial dissolution and precipitation in a more crystalline form is also occurring in the growing particles. It is worth noting that a consequence of this behaviour is that the nanoparticles experiencing ripening are not necessarily those having a bigger size but those which might be better crystallized in the "as deposited" state or a combination of both factors. Unfortunately, this point could not be assessed during the "*in situ*" SEM and global XRD experiments carried out in this work. Overall, this evidence portrays a complex situation where the surface to bulk energy ratio, commonly taken as the effective driving force of a classical Ostwald ripening process, must be complemented with differences in facets' energies and between partially amorphous and well crystallized OAD NaCl nanoparticles. Similar considerations have been claimed to explain differences in vaporization temperatures of NaCl nanocrystals depending on their size.[39] The implications of these findings can be of relevance to account for recrystallization and ripening phenomena in natural environments[20–22] or in harsh conditions or even in space[40] wherein partial amorphisation or unfavourable termination of small nanoparticles could provoke their spontaneous transformation under conditions enabling mass transport and particle regrowth.

Experimental

NaCl nanoparticles were deposited on a silicon (100) wafer by electron beam evaporation of pellets of this material (Sigma Aldrich). The substrates were placed at 60° and 85° oblique angles with respect to the evaporation source and separated from it by approximately 0.8 m. The deposition process was controlled with a calibrated quartz crystal monitor. For the reported experiments, 150 nm and 26 nm equivalent thickness of NaCl were selected for samples NaCl-60° and NaCl-85°, respectively.

Specimens were placed in an ESEM wherein both the water vapour pressure and the temperature were adjusted to induce

condensation while successively taking normal and cross-section micrographs, the latter after dicing the silicon substrates. The same specimens were also examined by XRD in a Bragg–Brentano configuration before and after their low temperature exposure to water vapour in the ESEM chamber. In parallel, we carried out an "*in situ*" XRD analysis with an environmental cell wherein the original sample was exposed at room temperature to water vapour at saturated conditions. The ESEM experiments were carried out in an FEI Quanta 250 FEG system working at 5 kV at a working distance of 6 mm from the surface. Precautions were taken to minimize any possible effect of the electron beam on the ripening process and adjustments were made in the dosage of electrons and scanning rate. Images were obtained while increasing the vapour pressure into the chamber and by adjusting their temperature with a Peltier device. The number of particles and average inter-particle distance and size has been determined by directly analysing the images using ImageJ, a National Institutes of Health (NIH) – sponsored image processing platform (http://www.ini.uzh.ch/~acardona/trakem2.html).

X-ray diffraction patterns in a Bragg–Brentano configuration were taken in a D8 Discover diffractometer (Bruker AXS). *In situ* XRD recrystallization experiments at room temperature upon exposure to saturated vapour pressure conditions at room temperature were carried out in a X'Pert Pro from Panalytical for X-ray angles <1°.

After preparation and during the transfer of samples from the ESEM to the XRD chambers the samples were kept in a desiccator to avoid possible effects of the humidity of the atmosphere. The stability of the samples during their manipulation in air for introduction into the ESEM or XRD chambers was checked by successive observations in a conventional SEM microscope.

Acknowledgements

The authors thank the Junta de Andalucía (Projects TEP8067 and P10-FQM-6900) and the MINECO (Projects CONSOLIDER CSD2008-00023, MAT2013-42900-P, MAT2013-40852-R, 201560E055 and RECUPERA 2020) for financial support.

References

1 H. Furedi-Milhofer, *Pure Appl. Chem.*, 1981, **53**(11), 2041–2055.
2 R. Boistelle and J. Astier, *J. Cryst. Growth*, 1988, **90**, 14.
3 S. C. Jain and A. E. Hughes, *J. Mater. Sci.*, 1978, **13**, 1611.
4 K. Glasner, F. Otto, T. Rump and D. Slepčev, *Eur. J. Appl. Math.*, 2009, **20**, 1.
5 I. C. K. Karl Glasner, *Interfaces and Free Boundaries*, 2009, 37.
6 S. K. Hait, S. P. Moulik and R. Palepu, *Langmuir*, 2002, **18**, 2471.
7 F. Wang, V. N. Richards, S. P. Shields and W. E. Buhro, *Chem. Mater.*, 2014, **26**, 5.
8 I. Lifshitz and V. Slezov, *Soviet Physics–JETP*, 1959, **8**, 331.
9 I. Lifshits and V. Slezov, *Sov. Phys. Solid State*, 1960, **1**, 1285.
10 I. Lifshitz and V. V. Slyozov, *J. Phys. Chem. Solids*, 1961, **19**, 35.
11 C. Wagner, *Z. Elektrochem.*, 1961, **65**, 581.
12 J. H. Yao, K. R. Elder, K. H. Guo and M. Grant, *Phys. Rev. B: Condens. Matter Mater. Phys.*, 1993, **47**, 14110.
13 M. Iggland and M. Mazzotti, *Cryst. Growth Des.*, 2012, **12**, 1489.
14 T. Vetter, M. Iggland, D. R. Ochsenbein, F. S. Hänseler and M. Mazzotti, *Cryst. Growth Des.*, 2013, **13**, 4890.
15 L. Ratke and P. W. Voorhees, *Growth and Coarsening: Ostwald Ripening in Material Processing*, Springer Science & Business Media, 2002.
16 H. Chun Zeng, *Curr. Nanosci.*, 2007, **3**, 177.
17 K. Biswas, N. Varghese and C. N. R. Rao, *J. Mater. Sci. Technol.*, 2009, **24**, 615.
18 W. Ostwald, *Studien Über Die Bildung Und Umwandlung Fester Körper. 1. Abhandlung: Übersättigung Und Überkaltung*, 1897.
19 J. S. Jahren, *Clay Miner.*, 1991, **26**, 169.
20 J. Warren, *Earth-Sci. Rev.*, 2000, **52**, 1.
21 M. Angeli, J. P. Bigas, D. Benavente, B. Menéndez, R. Hébert and ¡ C. David, *Environ. Geol.*, 2006, **52**, 205.
22 M. E. Wise, K. Baustian, T. Koop, M. A. Freedman, E. J. Jensen and M. A. Tolbert, *Atmos. Chem. Phys.*, 2012, **12**, 1121.
23 M. Salmeron, A. Verdaguer, J. J. Segura, J. Fraxedas and H. Bluhm, *J. Phys. Chem. C*, 2008, **112**, 16898.
24 K. Arima, P. Jiang, D. S. Lin, A. Verdaguer and M. Salmeron, *J. Phys. Chem. A*, 2009, **113**, 9715.
25 K. Arima, P. Jiang, X. Deng, H. Bluhm and M. Salmeron, *J. Phys. Chem. C*, 2010, **114**, 14900.
26 K. Yagi and G. Honjo, *J. Phys. Soc. Jpn.*, 1964, **19**, 1892.
27 M. M. Hawkeye, M. T. Taschuk and J. M. Brett, *Glancing Angle Deposition of Thin Films*, John Wiley & Sons, Ltd, 2014.
28 A. Barranco, A. Borras, A. R. Gonzalez-Elipe, A. Palmero, *Prog. Mater. Sci.*, 2016, **76**, 59.
29 L. G. Schulz, *J. Chem. Phys.*, 1949, **17**, 1153.
30 H. Bethge and K. W. Keller, *J. Cryst. Growth*, 1974, **23**, 105.
31 J. Yang, R. Dariani, C. Elliott, C. Buzea and K. Robbie, *Soc. Vac. Coat. 49th Annual Technical Conference Proceedings*, 2006, (505/856–7188) 689.
32 Y. He and Y. Zhao, *Nanoscale*, 2011, **3**, 2361.
33 L. González-García, J. Parra-Barranco, J. R. Sánchez-Valencia, A. Barranco, A. Borras, A. R. Gonzalez-Elipe, M. C. García-Gutierrez, J. J. Hernandez, D. R. Rueda and T. A. Ezquerra, *Nanotechnology*, 2012, **23**, 205701.
34 T. Karabacak, J. P. Singh, Y. P. Zhao, G. C. Wang and T. M. Lu, *Phys. Rev. B: Condens. Matter Mater. Phys.*, 2003, **68**, 125408.
35 A. Amassian, K. Kaminska, M. Suzuki, L. Martinu and K. Robbie, *Appl. Phys. Lett.*, 2007, **91**, 173114.
36 D. R. Lide, *CRC Handbook of Chemistry and Physics*, Internet Version, CRC Press, Boca Raton, FL, 2005, section 4, p. 160, http://www.hbcpnetbase.com.
37 P. A. Mulheran, *Modell. Simul. Mater. Sci. Eng.*, 1994, **2**, 1123.
38 P. Dandekar, Z. B. Kuvadia and M. F. Doherty, *Annu. Rev. Mater. Res.*, 2013, **43**, 359.
39 N. Kana, S. Khamlich, J. B. K. Kana and M. Maaza, *Surf. Rev. Lett.*, 2013, **20**, 1350001.
40 J. W. Mullin, *Crystallization*, Butterworth-Heinemann, Oxford, 4th edn, 2001, p. 193.

